Photovoltaic effect by vapor-printed polyselenophene

Photovoltaic Effect by Vapor-Printed Polyselenophene

Won Jun Jo[a], David C. Borrelli[a], Vladimir Bulović[b], Karen K. Gleason[a,*]

_____

[a]Department of Chemical Engineering, Massachusetts Institute of Technology, Cambridge, Massachusetts 02139, USA
[b]Department of Electrical Engineering and Computer Science, Massachusetts Institute of Technology, Cambridge, Massachusetts 02139, USA
*Corresponding author (E-mail: kkg@mit.edu)

_____

Abstract

Polyselenophene (PSe) donor layers are successfully integrated into organic photovoltaic devices (OPV) for the first time. Thin, patterned films of this insoluble semiconductor were fabricated using a vacuum-based vapor-printing technique, oxidative chemical vapor deposition (oCVD) combined with *in-situ* shadow masking. The vapor-printed PSe exhibits a reduced optical bandgap of 1.76 eV and enhanced photo-responsivity in the red compared to its sulfur containing analogue, polythiophene. These relative advantages are most likely explained by selenium's enhanced electron-donating character compared to sulfur. The HOMO level of PSe was determined to be at -4.85 eV. The maximum power conversion efficiency achieved was 0.4% using a bilayer heterojunction device architecture with C_{60} as the donor.

1. Introduction

Various solar energy conversion systems have emerged as promising candidates to establish a clean and sustainable energy network.[1-4] Organic solar cells have attracted great attention from the solar energy community due to their potential to enable lightweight, flexible, large-area and cost-effective photovoltaic technology.[5-11] It is essential for further improvements in efficiency to develop new materials carrying a combination of small bandgap, high dielectric constant, and high charge mobility.[12-16]

Previously, many studies focused on creating suitable polymer candidates by using selenophene-based homopolymers and copolymers.[17-23] While these studies found that the selenophene-based polymers are good hole transporting polymers with relatively long wavelength absorption,[17-23] the application of unsubstituted polyselenophene (PSe) has been quite limited. Unsubstituted polymers are known to be more stable because of their densely packed structures preventing oxygen permeation into the polymer bulk.[24,25] The study of PSe has been limited due to the lack of suitable synthetic methods to create high-quality thin films displaying high charge mobility and stable electrochemical behaviors.[26] However, our previous work successfully fabricating PSe films via oxidative chemical vapor deposition (oCVD) encourages the incorporation of PSe into photovoltaic devices.[13]

Unlike other standard methods, oCVD offers an attractive substrate-independent synthesis route to insoluble or infusible polymers as it is a solvent-free, vacuum-based technique.[13,27,28] It is able to synthesize and deposit conjugated polymers simultaneously on a wide range of substrates at low temperature (25 ~ 100 ˚C) in a controllable fashion applying *in-situ* shadow masking. Moreover, oCVD still maintains vacuum processing benefits, such as well-defined thickness control and uniformity, conformal coverage, parallel and sequential deposition, and inline convertibility with other standard vacuum processes (e.g., thermal evaporation).[13,27,28] Recently, this versatile technique has advanced materially in its

applicability to secure a facile path to the deposition of diverse semiconducting or conducting conjugated polymers. These polymers can play central roles in organic electronic and optoelectronic devices. [27]

Here, we report the photovoltaic effect by PSe, employing a novel, yet simple, vacuum-based vapor-printing technique, which represents a combination of oCVD process with shadow masking.[27] The resulting semiconducting PSe is applied into bilayer heterojunction solar cells as an electron donor with an electron accepting C_{60}. This study results in a maximum power conversion efficiency (η_p) of 0.4%, which is the first demonstration of PSe utilized for organic photovoltaics.

2. Experimental Section

2.1. Polyselenophene Depositions

When substrates were indium tin oxide (ITO) coated glasses for the photovoltaic device fabrication, the polymer film was prepared by the vapor printing method. Otherwise, the basic oCVD process without shadow masking was employed to prepare the polymer film. The custom-built oCVD reactor consists of a vacuum chamber connected to monomer inlet ports and an exhaust to a pump. At the bottom and top of the chamber, a heating crucible for an oxidant and an inverted stage for substrates are placed, respectively.

During the deposition, the reactor body and the chamber pressure were maintained at 80 ˚C and 150 mTorr, respectively. Iron(III) chloride ($FeCl_3$, 97%, Sigma–Aldrich) and selenophene (97%, Sigma–Aldrich) were used as the oxidant and monomer without any further purification. $FeCl_3$ was sublimed at 330 ˚C. Polymer film thickness was controlled by the deposition time. Vapor-phase selenphene monomer was introduced into the reactor from a monomer jar. The jar was maintained at 25 ˚C and a needle valve was used to render the

monomer vapor flow rate constant at around 1 sccm. After deposition, the films were rinsed in methanol (≥ 99.9%, Sigma–Aldrich) for 10 min to remove reacted oxidant.

2.2. Polymer Characterization

Fourier transform infrared (FTIR) measurements of PSe films on silicon wafers were performed on a Nexus 870, Thermo Electron Corp. spectrometer. The atomic compositions of the films were estimated by X-ray photoelectron spectroscopy (XPS) a PHI VersaProbe II (Physical Electronics). The film thicknesses were examined using a Veeco Dektak 150 surface profilometer. The sheet resistance of the films was measured with a Jandel four-point probe in air. Conductivity values were calculated using the measured sheet resistivity and thickness. Morphology analysis for PSe films were accomplished using an Agilent Technologies AFM in tapping mode with a Bruker Si cantilever having a tip frequency of 330 kHz. The UV–vis spectra of PSe films on bare glasses were gained utilizaing a Varian Cary 5000 UV–vis spectrophotometer. To evaluate absorption coefficient of the films, transmission and reflection spectra were measured. For the reflection spectra, a specular reflectance accessory and an Al standard reference mirror (ThorLabs) were used.

To identify the highest occupied molecular orbital (HOMO) level of the oCVD PSe, cyclic voltammetry (CV) were conducted in a standard three-electrode cell containing tetrabutylammonium hexafluorophosphate (0.1 M) in acetonitrile as the electrolyte under a nitrogen atmosphere. The PSe film on an ITO-coated glass Ag/AgNO3 (0.01 M in acetonitrile), a Pt mesh attached to a Pt wire worked as the working electrode, reference electrode, and counter electrode, respectively. Current-voltage data were collected at a scan rate of 100 mV s^{-1} with ferrocene/ferrocenium (Fc/Fc^{+}) redox couple to calibrate the Ag/Ag^{+} reference electrode, and analyzed with a 660D potentiostat (CH Instruments).

2.3. Device Fabrication and Characterization

The photovoltaic devices were fabricated on 75 nm patterned ITO-coated glasses (Thin Film Devices, 50Ω/sq), cleaned by solvents (2 x DI water, 2 x acetone, and 2 x isopropanol) followed by 30 s of O_2 plasma (100W, Plasma Preen, Inc.). As described above, PSe films having different thicknesses were simultaneously synthesized and deposited on the substrates via oxidative polymerization, and then rinsed in methanol for 10 min to remove reacted oxidant. After the oCVD photoactive donor layer deposition, C_{60} (99.9%, sublimed, Sigma–Aldrich), purified once by vacuum train sublimation, bathocuproine (BCP, from Luminescence Technology Corp.), and Ag (Alfa Aesar, 1–3 mm shot, 99.9999%) were thermally evaporated at a rate of 0.1 nm/s. C_{60} (20 ~ 40 nm), BCP (7.5 nm), and Ag (100 nm) were used as electron acceptor, exciton blocking layer, and cathode, respectively. The Ag cathode was deposited through a shadow mask for each device to obtain the well-defined device area, 1.21 mm^2, which is estimated from the overlapped area between Ag cathode and ITO anode.

Current density-voltage (J-V) measurements were conducted in nitrogen atmosphere, and recorded by a Keithley 6487 picoammeter. One sun of air mass 1.5 G (AM 1.5 G) irradiation (100 mW/cm^2) was generated by 1 kW xenon arc-lamp (Newport 91191) filtered by an AM 1.5G filter. The solar simulator intensity was estimated using a calibrated silicon photodiode. The external quantum efficiency (EQE) spectrum was recorded by a Stanford Research Systems SR830 lock-in amplifier. A focused monochromatic beam of variable wavelength light was provided by an Oriel 1 kW xenon arc lamp equipped with an Acton 300i monochromator and chopped at 43 Hz. The incident monochromatic light intensity was evaluated using a Newport 818-UV calibrated silicon photodiode.

3. Results and Discussion

3.1. Polyselenophene synthesis and characterization

Based on a previous study, PSe is simultaneously synthesized and deposited on a variety of substrates from vapor-phase selenophene monomer and sublimed $FeCl_3$ oxidant.[13] The overall oxidative polymerization with sublimated $FeCl_3$ is illustrated in **Fig. 1**. Over oxidation makes the polymer conductive, the final state in **Fig. 1**, by forming polarons and bipolarons.[29] As shown above, the oCVD process results in the conductive blue PSe film, where cations are charge balanced by counter anions. The conductivity of the doped PSe film was evaluated to be from 2.6 (104.7 nm) to 35.4 S/cm (181.5 nm), roughly proportional to the film's thickness.

A methanol-rinse treatment causes the film to become semiconducting and go through an immediate color change to red. The conductivity of the PSe after rinsing was below the detection limit of the measurement system ($< 10^{-4}$ S/cm). The observed changes in conductivity and color are entirely consistent with previous reports, and indicate the rinsing treatment dedopes the oCVD PSe.[13,28] The dedoped state of the PSe is further confirmed by XPS atomic composition measurement. The rinsed PSe film does not have any elements (Fe and Cl) from the oxidizing agent, but includes C and Se at a ratio of 5.7 to 1. The FTIR spectrum of the rinsed PSe film in **Fig. 2a** also matches well with an earlier reported result.[13] Morphology of the rinsed PSe film was investigated using AFM. As **Fig. 2b** illustrates, oCVD-processed PSe surface is not completely flat, but has an acceptable level of roughness. Specifically, the root mean square (RMS) roughness value is 17.0 nm.

3.2. Energy level alignment

The UV-Vis absorption spectrum in **Fig. 2c** reveals that the onset of optical absorption by PSe appears at 705 nm, corresponding to the optical bandgap of 1.76 eV. To determine the HOMO level of PSe, cyclic voltammetry (CV) was used according to the standard three-electrode setup as described in the supporting information. The resulting CV curve for PSe is shown in **Fig. 3a**. Based on the curve, the HOMO level is located following previously stated procedures.[28,30] The onset of the oxidation peak is -0.25 V vs Fc/Fc^+. The HOMO is then

calculated by the following equation, assuming the redox potential of Fc/Fc^+ is – 5.1 eV relative to vacuum.[30, 31]

$$E_{HOMO} = -\{E_{\left[oxidation\ onset\ vs\frac{Fc}{Fc}+\right]} + (5.1 \pm 0.1)\}\ (eV) \quad (1)$$

The calculated HOMO level is -4.85 ± 0.1 eV, and the lowest unoccupied molecular orbital (LUMO) level of PSe is determined to be -3.09 ± 0.1 eV by adding the optical bandgap of 1.76 eV to the HOMO. Taking the estimated HOMO and LUMO into account, the energy level diagram of PSe solar cells is drawn in **Fig. 3b**.

3.3. Photovoltaic device performance

To investigate the photovoltaic effect by vapor-printed PSe, we employed a single bilayer heterojunction architecture, as demonstrated in **Fig. 4**, consisting of the ITO anode substrates, electron donating PSe, electron accepting C_{60}, exciton blocking BCP, and top capping Ag cathode. We also explored a range of thicknesses of the C_{60} and PSe layers to further understand how the two layers affect the device performance as well as to optimize that. **Fig. 5** displays how the performance varies with C_{60} layer thickness under the fixed PSe layer thickness (70 nm). The optimum C_{60} layer thickness is 30 nm, a finding in agreement with a previous report.[28]

The change in short-circuit current (J_{SC}) with C_{60} layer thickness is mainly due to the variation in optical interference patterns within the device, as the reflective Ag interface moves along with C_{60} layer thickness.[32] For example, the reflective interface is displaced farther from the PSe/C_{60} interface with increasing C_{60} layer thickness. Considering the device architecture, the optical electric field for shorter wavelengths matched with C_{60} absorption peak is expected to be maximized closer to the reflective interface, whereas the field for longer wavelengths corresponding to PSe absorption peak is likely to reach its peak farther from the interface. In this sense, the alteration in C_{60} layer thickness should have an impact on

the optical electric field distribution inside the device and thus exciton generation in the C_{60} and PSe layers, closely linked to J_{SC}.

The representative J-V curves for varying PSe layer thicknesses are shown in **Fig. 6a**. The optimized device with 60 nm PSe and 30 nm C_{60} layers exhibits η_p = 0.4%, open-circuit voltage (V_{OC}) = 0.554 V, J_{SC} = 2.18 mA/cm^2, and fill factor (FF) = 0.33. OPVs utilizing polythiophene, PSe's sulfur-containing analogue, by oCVD were previously studied.[27] It should be noted that the best PSe layer thickness (60 nm) is much thicker than oCVD polythiophene's optimal thickness (25 nm).[28] A comparison of PSe's absorption coefficient (α_{PSe}) with polythiophene's (α_{PT}) illuminates why there is the difference in the optimum thickness. As **Fig. 6b** depicts, while α_{PSe} is slightly higher than α_{PT} for longer wavelengths than 625 nm, α_{PSe} is significantly lower than α_{PT} in the other region. This suggests PSe film should be thicker than PT film to obtain sufficient light absorption for exciton generation, which is supported by Beer-Lambert equation.

However, the increase in the polymer layer thickness must have a negative impact on hole diffusion, as holes must go through the longer path from the donor-acceptor interface after charge separation in order to be collected by anode. The longer path can cause more holes to be extinguished during the hole diffusion since oCVD PSe with imperfect regioregularity is likely to have a relatively low hole mobility. It is strongly associated with a rise in series resistance (R_S) with increasing PSe layer thickness, observed as a lower slope at V_{OC} in the J-V curves of **Fig. 6a**. The correlation between R_S and exciton-generating polymer layer thickness is also supported by an previous study.[28] Generally, each semiconducting polymer has a different level of trade-off between exciton generation from optical absorption and hole diffusion, deteriorating with a longer diffusion path, based on its own α, bandgap, and charge mobility. For PSe, 60 nm is the optimum thickness striking a balance between exciton generation and hole diffusion.

The EQE spectrum was measured for the optimized PSe photovoltaic device (filled circles). The spectrum in **Fig. 6c** makes it clear how photocurrent is related to incident photon by the device quantum efficiency. Notably, the spectrum shape is well-matched with a combination of α curves of PSe and C_{60}, which confirms the photocurrent originates from photon to electron conversion by PSe and C_{60}. To attain more systematic understanding of oCVD PSe's photo-responsivity, the EQE of the PSe device is compared with that of polythiophene (PT) solar cells (open circles), adopted from our previously published data.[28] As shown in **Fig. 6c**, the PSe device exhibits a broader EQE spectrum with pronounced shoulder at 610 nm than the PT device does, which suggests oCVD PSe is more photo-sensitive in the red than oCVD PT. It is coherent with the comparison of α_{PSe} and α_{PT} in **Fig. 6b** as well as EQE spectrum distribution patterns established by poly(3-hexylselenophene) research.[33] However, the maximum EQE by PSe is smaller than that by PT. It is most likely explained by longer exciton diffusion length and more regiochemical defects of oCVD PSe compared to oCVD PT. The regiochemical defects of oCVD PSe is discussed in detail in the next section.

3.4. Regiochemical defects in oCVD polyselenophene

As regioregularity of semiconducting polymers is closely connected to their charge mobility, the more regioregular, the better for photovoltaic performance by realizing smaller R_S and thus larger FF.[5,19,33] According to our preceding research, the main difference between PSe and PT photovoltaic devices is FF in terms of performance parameters.[28] In other words, oCVD PSe could be less regioregular than oCVD PT. In order to gain insights into the difference in regioregularity between oCVD PSe and PT, selenium's ionization energy (IE) and sulfur's IE are compared since IE is an important chemical property affecting oxidative polymerization mechanisms.

Selenium has the lower IE (941 kJ/mole) than sulfur (999.6 kJ/mole) because selenium is in the 4th row of the periodic table and thus holds more valence electrons farther from the atomic nucleus than its 3rd row analogue. This indicates when selenophene is oxidized into a radical intermediate to initiate oxidative polymerization, selenium's smaller IE could render the intermediate more stable. As a result, the intermediate has an increased chance for radical migrations from carbon 2 (or 5) to carbon 3 (or 4). If the radical migrations occur, the final product, polyselenophene, should have regiochemical defects, degrading charge mobility, R_S, FF, and η_p sequentially. (See **Fig. 7** for more details).

The regionchemical defects were actually identified by FTIR analysis. The sharp FTIR peak (~ 790 cm^{-1}) and the broad FTIR peak (~ 830 cm^{-1}) in **Fig. 2a** correspond to α-α' coupling (i.e., regioregular structure in polymer chain) and α-β coupling (i.e., regiochemical defects in polymer chain), respectively. Hence, the replacement of sulfur by selenium has a negative influence on the regioregularity of oCVD-processed polymer, whereas the enhanced electron donating capability of selenium provides PSe with higher dielectric constant and smaller bandgap than those of PT.

4. Conclusion

As oCVD enables insoluble and infusible polyselenophene to be incorporated into bilayer heterojuction photovoltaic devices with C_{60}, we were able to demonstrate polyselenophene's photovoltaic effect with a maximum η_p of 0.4% for the first time using the novel, yet simple, vacuum-based vapor-printing technique. Vapor-printed polyselenophene exhibits the reduced optical bandgap of 1.76 eV as well as enhanced photo-responsivity in the red in comparison with its analogue, polythiophene. These relative advantages are most likely due to selenium's electron-donating nature, but this characteristic also causes selenium to have lower ionization energy than sulfur. As a result, more regiochemical defects form within oCVD polyselenophene than in oCVD polythiophene, which is ultimately disadvantageous for η_p.

This is a remaining issue limiting the η_p of the polyselenophene solar cells.

Acknowledgements

This work was supported by Eni SpA under the Eni-MIT Solar Frontiers Center and by a Samsung fellowship from the Samsung Foundation of Culture and a National Science Foundation Graduate Research Fellowship. This work was also supported in part by the U.S. Army Research Laboratory and the U.S. Army Research Office through the Institute for Soldier Nanotechnologies, under contract number W911NF-13-D-0001. W.J.J. thanks Dr. Y.S. Lee for insightful discussions.

References

[1] M. Grätzel, *Inorg. Chem.* 2005, *44*, 6841.

[2] T. R. Cook, D. K. Dogutan, S. Y. Reece, Y. Surendranath, T. S. Teets, D. G. Nocera, *Chem. Rev.* 2010, *110*, 6474.

[3] M. G. Walter, E. L. Warren, J. R. McKone, S. W. Boettcher, Q. Mi, E. A. Santori, N. S. Lewis, *Chem. Rev*. 2010, *110*, 6446.

[4] W. J. Jo, J.-W. Jang, K. Kong, H. J. Kang, J. Y. Kim, H. Jun, K. P. S. Parmar, J. S. Lee, *Angew. Chem. Int. Ed.* 2012, *51*, 3147.

[5] B. C. Thompson, J. M. J. Frechet, *Angew. Chem. Int. Ed.* 2008, *47*, 58.

[6] R. D. McCullough, *Adv. Mater.* 1998, *10*, 93.

[7] C. J. Brabec, S. Gowrisanker, J.J.M. Halls, D. Laird, S.J. Jia, S.P. Williams, *Adv. Mater.* 2010, *22*, 3839.

[8] E. Bundgaard, F. C. Krebs, *Sol. Energ. Mat. Sol. C*. 2007, *91*, 954.

[9] S.R. Forrest, *Nature* 2004, *428*, 911.

[10] J. You, L. Dou, K. Yoshimura, T. Kato, K. Ohya, T. Moriarty, K. Emery, C.-C. Chen, J. Gao, G. Li, Y. Yang, *Nat. Commun.* 2013, *4*, 1446.

[11] 12.0% efficienct vacuum-deposited organic small molecular solar cells (Heliatek), www.heliatek.com/newscenter/latest_news/neuer-weltrekord-fur-organische-solarzellen-heliatek-behauptet-sich-mit-12-zelleffizienz-als-technologiefuhrer/?lang=en, accessed: April, 2014.

[12] D. C. Watter, H. Yi, A. J. Pearson, J. Kingsley, A. Iraqi, D. Lidzey, *Macromol, Rapid Commun.* 2013, *34*, 1157.

[13] D. Bhattacharyya, K. K. Gleason, *J. Mater. Chem.* 2012, *22*, 405.

[14] L. J. A. Koster, S. E. Shaheen, J. C. Hummelen, *Adv. Energy Mater*. 2012, *2*, 1246.

[15] R. C. Chiechi, J. C. Hummelen, *ACS Macro Lett*. 2012, *1*, 1180.

[16] N. Camaioni, R. Po, *J. Phys. Chem. Lett.* 2013, *4*, 1821.

[17] D. S. Chung, H. Kong, W. M. Yun, H. Cha, H.-K. Shim, Y.-H. Kim, C. E. Park, *Org. Electron.* 2010, *11*, 899.

[18] D. J. Crouch, P. J. Skabara, M. Heeney, I. McCulloch, D. Sparrowe, S. J. Coles, M. B. Hursthouse, *Macromol. Rapid Commun.* 2008, *29*, 1839.

[19] M. Heeney, W. Zhang, D. J. Crouch, M. L. Chabinyc, S. Gordeyev, R. Hamilton, S. J. Higgins, I. McCulloch, P. J. Skabara, D. Sparrowe, S. Tierney, *Chem. Commun.* 2007, *47*, 5061.

[20] H. Kong, D. S. Chung, I.-N. Kang, J.-H. Park, M.-J. Park, I. H. Jung, C. E. Park, H.-K. Shim, *J. Mater. Chem.* 2009, *19*, 3490.

[21] Y. Kunugi, K. Takimiya, K. Yamane, K. Yamashita, Y. Aso, T. Otsubo, *Chem. Mater.* 2003, *15*, 6.

[22] D. Gao, J. Hollinger, D. S. Seferos, *ACS Nano*, 2012, *6*, 7114.

[23] J. Hollinger, J. Sun, D. Gao, D. Karl, D. S. Seferos, *Macromol. Rapid Commun.* 2013, *34*, 437.

[24] F. C. Krebs, H. Spanggaard, *Chem. Mater.* 2005, *17*, 5235.

[25] S. A. Gevorgyan, F.C. Krebs, *Chem. Mater.* 2008, *20*, 4386.

[26] A. Patra, M. Bendikov, *J. Mater. Chem.* 2010, *20*, 422.

[27] A. M. Coclite, R. M. Howden, D. C. Borrelli, C. D. Petruczok, R. Yang, J. L. Yagüe, A. Ugur, N. Chen, S. Lee, W. J. Jo, A. Liu, X. Wang, K. K.Gleason, *Adv. Mater.* 2013, *25*, 5392.

[28] D. C. Borrelli, M. C. Barr, V. Bulović, K. K. Gleason, *Sol. Energ. Mat. Sol. C.* 2012, *99*, 190.

[29] T. A. Skotheim, R. L. Elsenbaumer, J. R. Reynolds, *Handbook of Conducting Polymers*, Marcel Dekker, Inc., New York 1998, p. 225.

[30] C. M. Cardona, W. Li, A. E. Kaifer, D. Stockdale, G. C. Bazan, *Adv. Mater.* 2011, *23*, 2367.

[31] B. W. D'Andrade, S. Datta, S. R. Forrest, P. Djurovich, E. Polikarpov, M. E. Thompson, *Org. Electron*. 2005, *6*, 11.

[32] P. Peumans, A. Yakimov, S. R. Forrest, *J. Appl. Phys.* 2003, *93*, 3693.

[33] A. M. Ballantyne, L. Chen, J. Nelson, D. D. C. Bradley, Y. Astuti, A. Maurano, C. G. Shuttle, J. R. Durrant, M. Heeney, W. Duffy, I. McCulloch, *Adv. Mater.* 2007, *19*, 4544.

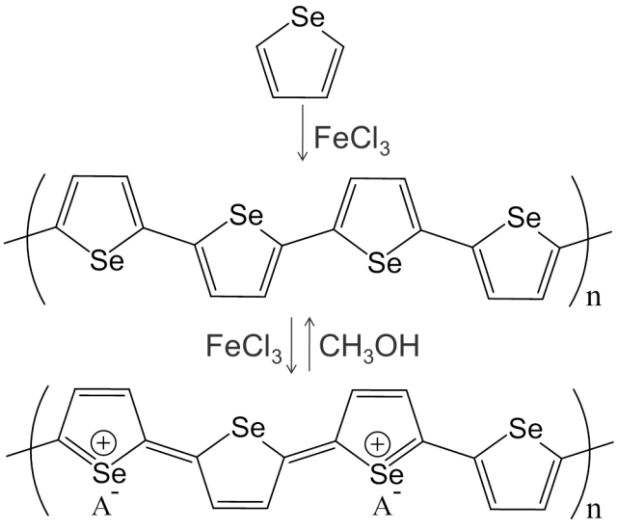

Fig. 1. Synthetic route from selenophene to polyselenophene via oCVD.

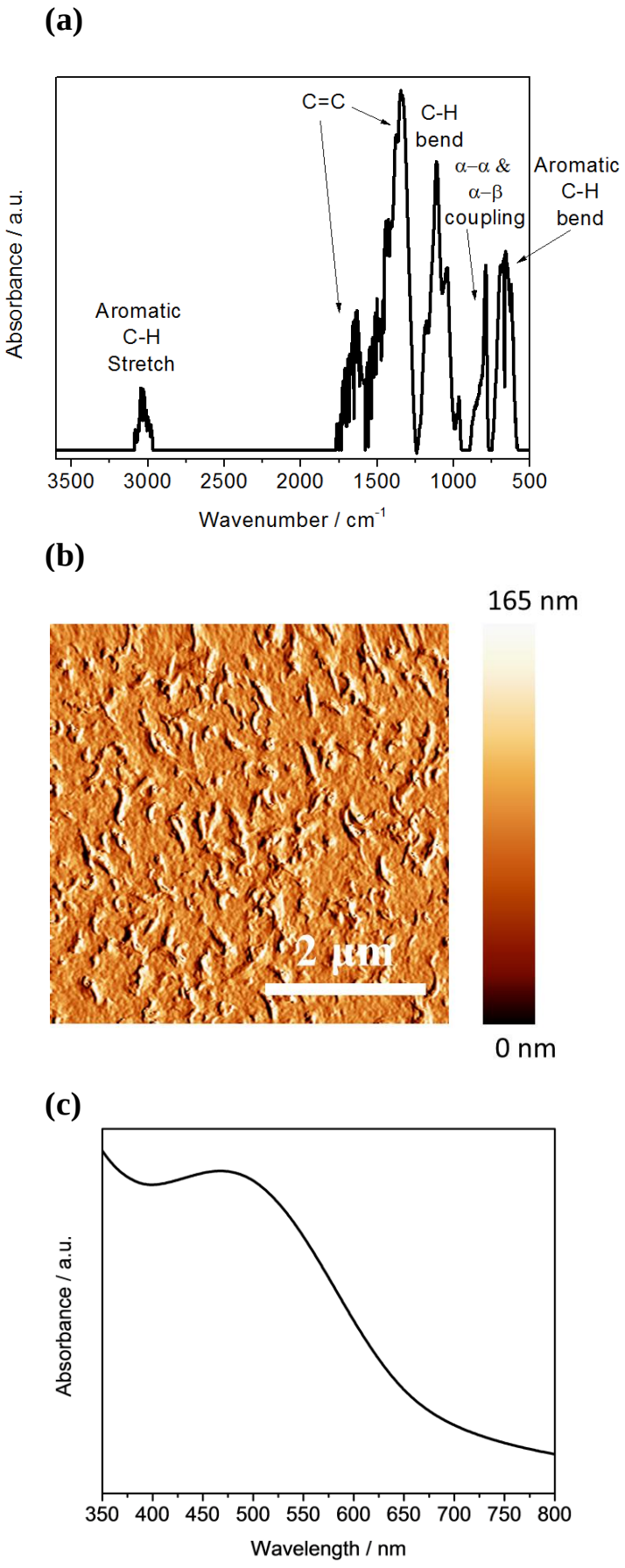

Fig. 2. (a) FTIR spectrum (b) AFM topography image (c) UV-Vis absorption spectrum of oCVD polyselenophene film

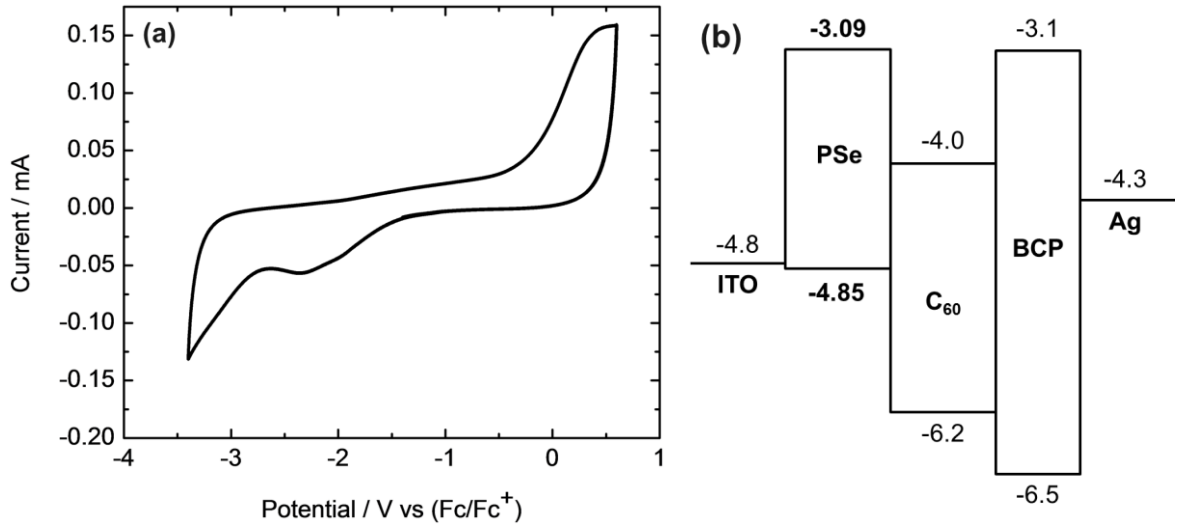

Fig. 3. (a) Cyclic voltammetry of oCVD polyselenophene film on an ITO electrode. (b) Schematic energy level alignment of oCVD polyselenophene solar cells.

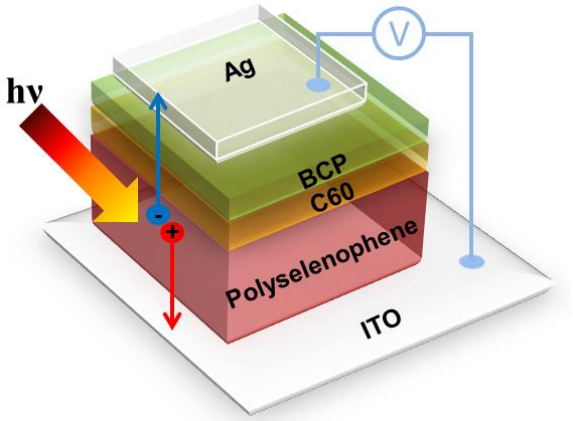

Fig. 4. Single bilayer heterojunction architecture of oCVD polyselenophene solar cells

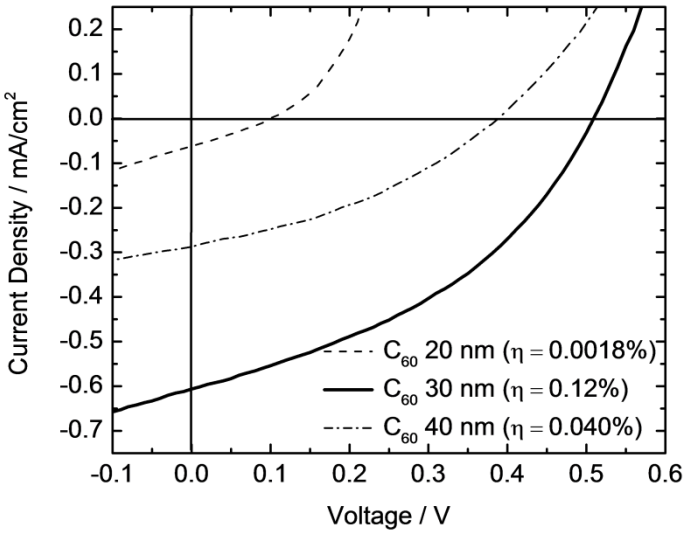

Fig. 5. Representative J-V curves for varying C_{60} thickness with 70 nm of oCVD polyselenophene layer.

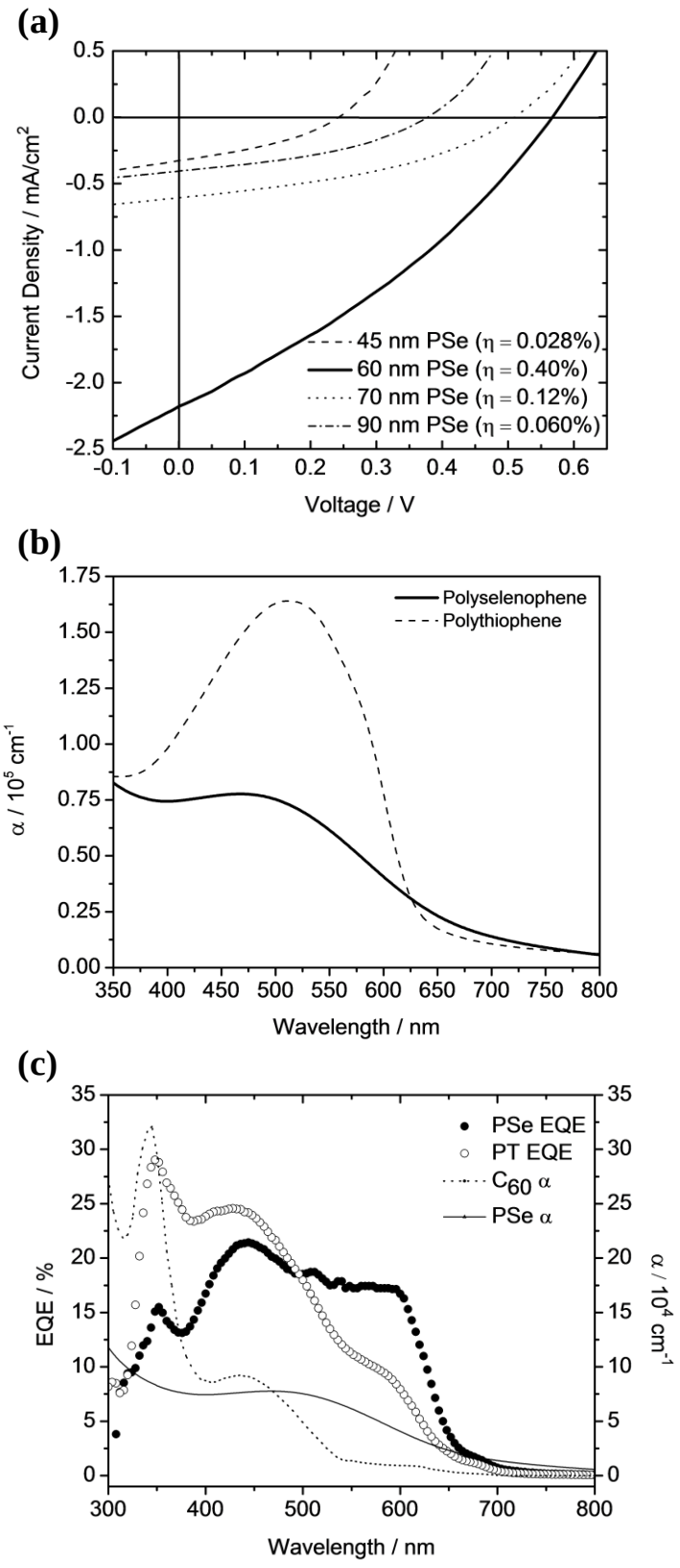

Fig. 6. (a) Representative J-V curves for varying polyselenophene layer thickness with 30 nm of C_{60}, (b) Comparison of absorption coefficients of oCVD polyselenophene and oCVD polythiophene. (c) EQE spectra of representative photovoltaic devices using oCVD polythiophene and polyselenophene, and absorption coefficients of oCVD polyselenophene and C_{60}.

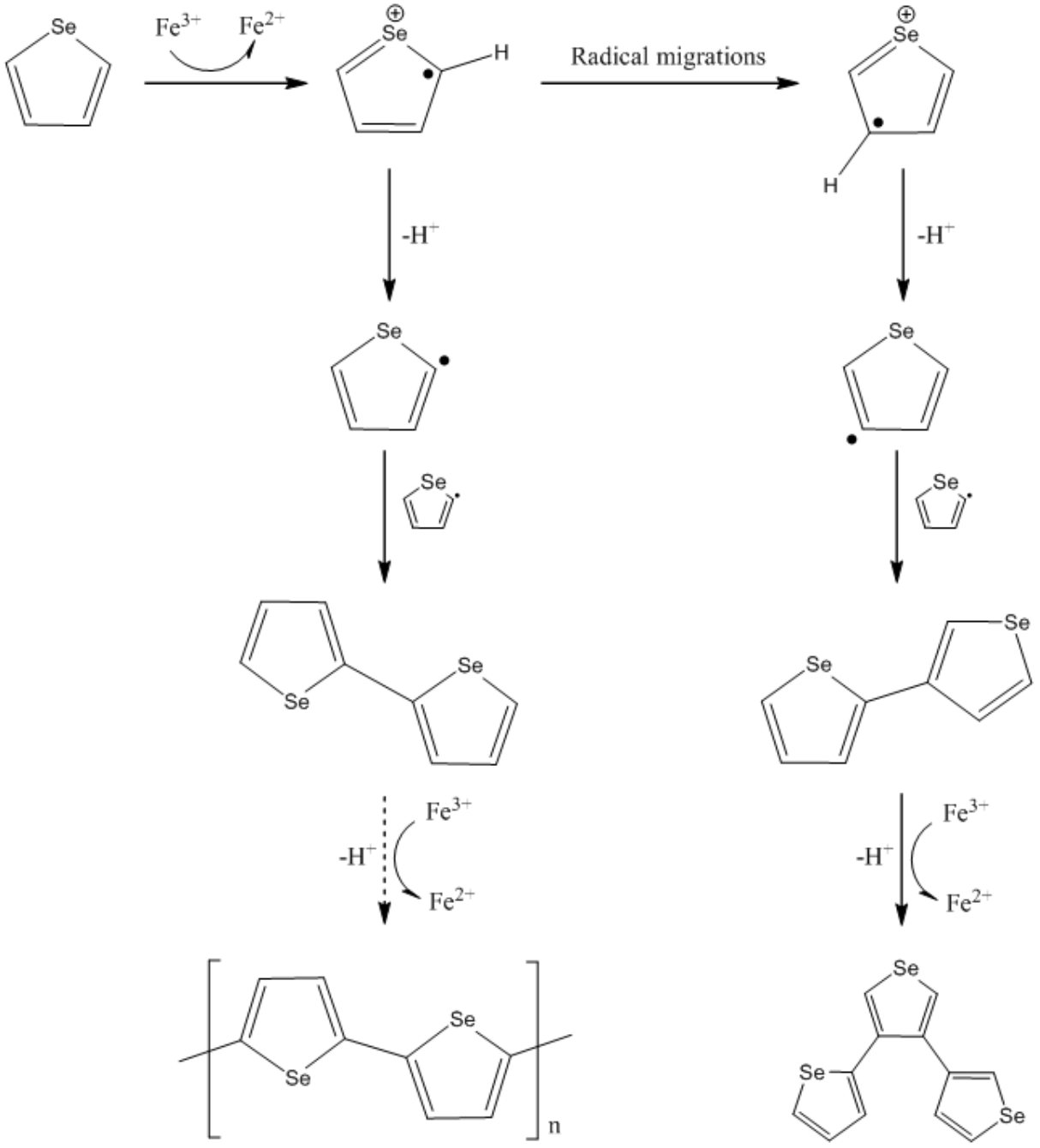

Fig. 7. Regiochemical defects within oCVD polyselenophene caused by radical migrations.